A predictive model for fracture in human ribs based on in-vitro Acoustic Emission Data

S. García-Vilana[a]*, D. Sánchez-Molina[a],
J. Llumà[b], I. Fernández-Osete[c]
J. Veláquez-Ameijide[a], E. Martínez-González[c]

June 16, 2021

[a]UPC, RMEE-GRABI, Eduard Maristany, 14, 08036 Barcelona
[b]UPC, CFM-GRABI, Eduard Maristany, 14, 08036 Barcelona
[c]UPC, EM-LEAM, Eduard Maristany, 14, 08036 Barcelona

Abstract

Purpose. The aim of this paper is to propose a fracture model for human ribs based on Acoustic Emission (AE) data. The accumulation of micro-cracking until a macroscopic crack is produced can be monitored by AE. This macro-crack propagation causes the loss of the structural integrity of the rib.

Methods. The AE technique was used in in-vitro bending tests of human ribs. The AE data obtained were used to construct a quantitative model that allows an estimation of the failure stress from the signals detected. The model predicts the ultimate stress with an error of less than 3.5% (even at stresses 15% lower than failure stress), which makes it possible to safely anticipate the failure of the rib.

Results. The Percolation Theory was used to model crack propagation. Moreover, a quantitative probability-based model for the expected number of AE signals has been constructed, incorporating some ideas of percolation theory. The model predicts that AE signals associated with micro-failures should exhibit a vertical asymptote when stress increases. The occurrence of this vertical asymptote

*Corresponding author: silvia.garcia.vilana@upc.edu

was attested in our experimental observations. The total number of micro-failures detected prior to the failure is $N \approx 100$ and the ultimate stress is $\sigma_\infty = 197 \pm 62$ MPa. A significant correlation ($p < 0.0001$) between σ_∞ and the predicted value is found, using only the first $N = 30$ micro-failures (correlation improves for N higher).

Conclusions. The measurements and the shape of the curves predicted by the model fit well. In addition, the model parameters seem to explain quantitatively and qualitatively the distribution of the AE signals as the material approaches the macroscopic fracture. Moreover, some of these parameters correlate with anthropometric variables, such as age or BMI. The proposed model could be used to predict the structural failure of ribs subjected to bending.

KEYWORDS: Acoustic Emission, Biomechanics, Human Rib, Probabilistic models, Percolation.

1 Introduction

The prediction of bone fracture under stress is a problem of practical interest. Recently, some medical imaging techniques have been developed to estimate the degree of deformation of a bone based on medical images [1]. This, coupled with computationally adequate constitutive models, provides a potential method for predicting the strength capacity of bone. However, there is still considerable uncertainty about the accuracy of such methods. For example, some studies have attempted to evaluate the accuracy of computational models for predicting fracture value, finding that the value predicted by Finite Element Model (FEM)-based simulations can contain errors that range from 5 to 46% [2], a considerable magnitude. Therefore, given the current state of the art in medical imaging technology and the reliability of bone computational models, it is interesting to explore other approaches of work. Other empirical techniques such as Acoustic Emission (AE) can be used to detect the growth of incipient micro-failures, which could potentially be applied to *in vivo* monitoring of bone under stress [3, 4, 5].

The AE technique has been previously used in the biomedical field, showing its wide range of applications. In the field of orthopedics, for example, AE has been used for implant design, failure prediction or even orthopedic diagnosis [6, 7]. In the latter approach, it has been shown that AE can even determine the appropriate time for the removal of external fixations in bone healing before radiographic diagnosis [8].

The AE technique has been extensively used in different materials for real-time monitoring [9, 10], including biological materials [11, 12]. However, the literature on AE in human bones is less extensive and has been limited to the description of the emission release pattern and the study of the signal increase with load [5, 13, 14]. Some other studies analyzed the loading process of specific bones such as the femur or the tibia [14, 15, 16, 17], but most of these studies focused on the monitoring of damage under increasing load [18], and also on the influence of age and the distribution of energies and amplitudes of the recorded signals [19, 20]. In most cases, no specific models have been outlined to describe the appearance of AE signals as stress increases. The model presented in this study is an attempt to fill this gap. In the framework of biomechanical applications, some research has used the AE technique for the analysis of fracture of bone and other biological materials; however, there are few quantitative models which use AE data for the prediction of fracture [21, 22, 23]. Moreover, these predictive models were developed for soft collagenous tissues, which makes them unsuitable for application in hard tissue (bone).

Using the AE technique and an appropriate quantitative model, it may be possible to estimate failure stress with some anticipation of its occurrence. However, a large part of the available studies of AE in the context of biomechanics are excessively empirical and are limited to descriptive comparisons. In fact, many of these studies focus either on the comparison of AE signals between specimens [11], or on the qualitative description of the region where AE signals are predominant in the force-deflection curve of bone [5, 16], or on the number of signals and their amplitude variation as a function of the strain rate [19]. Therefore, it seems necessary to develop quantitative fracture models for an estimation of the failure stress prior to fracture. Based on the aforementioned ideas, this work proposes such a model based on *in vitro* data with whole human ribs subjected to bending.
The main ideas of the model of this study are based on Percolation Theory. Even though the Percolation Theory has already been used in theoretical biomechanical models of bone fracture [24, 25, 26], no study has used the percolation theory statements along with AE data in the biomechanical field. Other studies, however, were developed in soil mechanics and fracture prop-

agation in rock materials, with models based on the principles of Percolation Theory to model crack propagation with AE data [27].

2 Data and Methods

The materials used in this study consisted of fresh human rib specimens harvested from forensic autopsies conducted at the Forensic Pathology Service of the Legal Medicine and Forensic Science Institute of Catalonia (FPS/IMLCFC). All the specimens were initially removed for complementary medical-legal investigation. This study was approved by the Research and Ethics Committee of the IMLCFC. Fifteen healthy 4th ribs were obtained from autopsies of ten *post mortem* human subjects (PMHS). Each complete rib was subjected to a three-point bending test and was loaded to complete fracture. In the bending tests, the AE technique described in section 2.1 was incorporated. Prior to the experimental tests, the soft tissue and cartilage were removed.

2.1 Acoustic Emission

The AE is a Non-Destructive Testing (NDT) technique used for the detection of elastic waves spreading in the material. The waves are generated by the release of elastic energy during the micro-cracking process: "There is a sudden drop in stress from the original level to zero on the new crack surface area when the crack jumps; this causes the radiation of elastic waves" [28]. The AE measurements consists in the placement of small sensors on the specimen that detect the elastic waves released in the material, during the succession of jumps spreading micro-cracks [28], usually grouped in avalanches, until macroscopic failure occurs (Figure 1) [20]. The signals exceeding the energy threshold are considered micro-cracking signals or *hits*, as it has been verified in collagenous tissues when fibers fail [21].

In this study, it is assumed that the progression of micro-cracks in the inter-osteon space produces most of the detected AE signals: when the micro-cracks produced near the maximum stress converge, they produce a continuous macro-crack that eventually nucleates a macroscopic crack. In addition, it is assumed that when a bond (or set of bonds) within the osteon network goes from intact state to broken state, an AE signal is produced, and the breaking process could be modeled by Percolation Theory with non-independent bond breaking probability associated to the stress field (see sec-

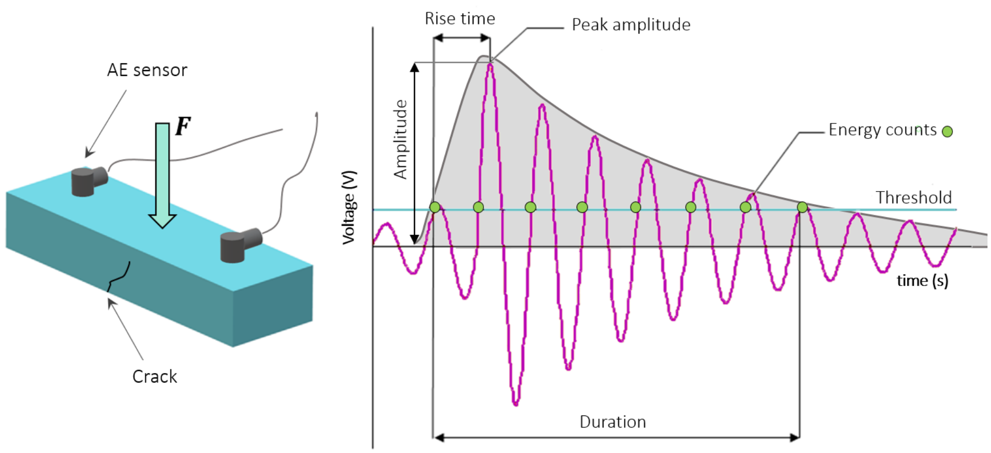

Figure 1: (a) AE technique, (b) Main AE wave features. Threshold discriminates the noise or disturbing signals and energy (gray area) is computed by means of the amplitude, count and duration parameters.

tion 2.3).

2.2 Experimental Setting

The human ribs were tested with a specific methodology that allows for frictionless sliding of the ends of the rib. This setting can be used to determine the deflections and displacements at any point of the rib. The entire ribs were subjected to three-point bending tests, as can be seen in Figure 2. This configuration for the tests allows a sliding and opening of ends of the rib, then the use of Digital Image Correlation (DIC) makes it possible to compute the displacements along the rib from which to calculate the strain. In addition, the stress can be computed from the measured force and the geometrical cross-sectional properties along the rib.

Bending tests were performed with a ZwickRoell® Proline 7.1 and a load cell HBM®. A U-shaped guide was placed on the upper platform into which the rib extremes were inserted (the rib was contained in the machine plane). The guide was covered with lubricant and the rib ends were wrapped with polytetrafluoroethylene band to ensure a sliding and to minimize the friction. On the lower platform, a base was fixed in which the impactor was attached (see Figure 2). The impactor exerted the force on the central external region of the rib. The base supported four safety bars to prevent possible slippery

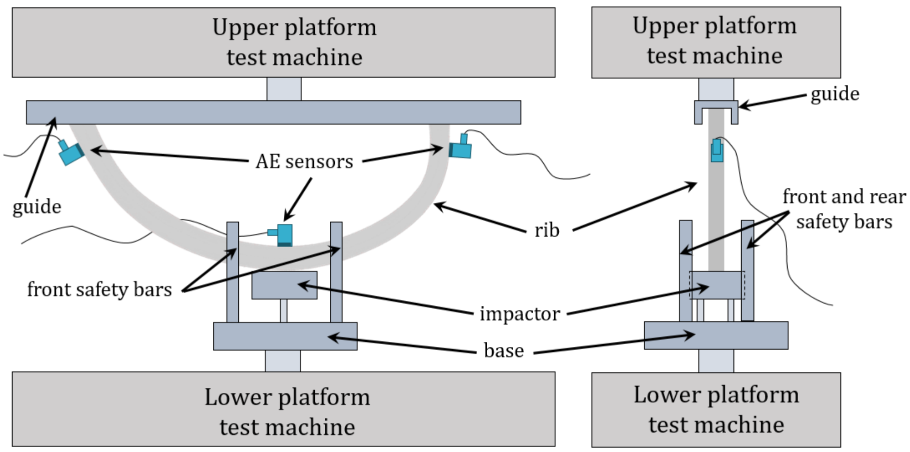

Figure 2: Experimental setting: the rib is placed with its extremes inside the guide and the outer central region in contact with the impactor. An AE sensor is placed in the central region where the main fractures occur along with two sensors placed near the ends to discriminate friction signals.

of the rib during the test (the bars were never in contact with the rib). The whole test was recorded with a high-speed camera (PCO 1200s) and from the sequence of video frames, the displacements on the rib during the test were determined following a DIC procedure with MATLAB®. From displacements and force, strain and stress on the fracture region of each rib were obtained during the whole test.

For the computations of the stress, the axial force N_x and the bending moment M_z in the fracture cross-section was determined for each time during the test and with these values, the stress was calculated by means of the Navier's formula [29]:

$$\sigma(t) = \frac{N_x(t)}{A} - \frac{yI_{yy} - zI_{yz}}{I_{yy}I_{zz} - I_{yz}} M_z(t) \tag{1}$$

where I_{yy}, I_{zz} are the second moments of area, I_{yz} the product moment of area and y, z the vertical and horizontal distances from the centroid of the fractured section to the bottom point of the rib where the maximum stresses occur. These magnitudes were determined from rib CT images, from which the geometric area magnitudes necessary for the application of the formula (1) could be calculated.

Prior to the test, three resonant AE sensors (VS700-D, Vallen System

Gmbh) were placed along the rib; two sensors at the ends to discriminate friction signals and another sensor in the inner central region of the rib, where greater stresses and macroscopic fracture occur. Three AE amplifiers (AEP4) were used, together with a four channel system (AMSY-5) and a band-pass filter between 25–1100 kHz to discriminate noise or possible friction signals.

A lighting system was installed in the camera and its voltage was connected to both force and AE acquisition systems. Prior to the force increase, the light was interrupted for a very short time, and the acquisition systems recorded null voltages during this time. Thus, based on the recorded voltage drop and the video light switch-off, forces, displacements and AE signals were synchronized, with a precision better than 10 ms.

2.3 Model based in Percolation Theory

The cortical bone is constituted by an aggregate of quasi-cylindrical units called osteons, consisting of mineral lamellae and collagen fibers that surround the Havers canal. Osteons are mainly aligned along the longitudinal axis of long bones and the boundary between osteons is composed by the cement lines and interstitial bone [30]. Thus, in a cross-section to the axis of the bone, the cortical bone approaches to a set of circle-like structures corresponding to the osteons, embedded in the matrix (interstitial bone and cement lines).

The process of micro-cracking in the bone osteon network has been addressed in the literature. Previous studies suggest that osteons act as a barrier in the propagation of micro-cracks, which would preferably occur along the cement lines and interstitial tissue, promoting the separation of osteons [31, 32, 33, 34]. Thus, it can be assumed that cortical bone is formed by a net of basic cells that represent the osteons and whose limits or bonds correspond to the cement lines and interstitial tissue. The micro-cracks preferably propagate between osteons (see Figure 3), which implies the cracking of the mesh bonds, and this propagation implies an energy release as an AE signal. Therefore, an increase in the load applied to the bone means an increase in the number of cracked bonds in the mesh, and macroscopic fracture occurs when a set of bonded cracked bonds crosses the net completely.

The prediction of the propagation and bonding of cracked bonds up to macroscopic fracture can be studied by the Percolation Theory of bonds

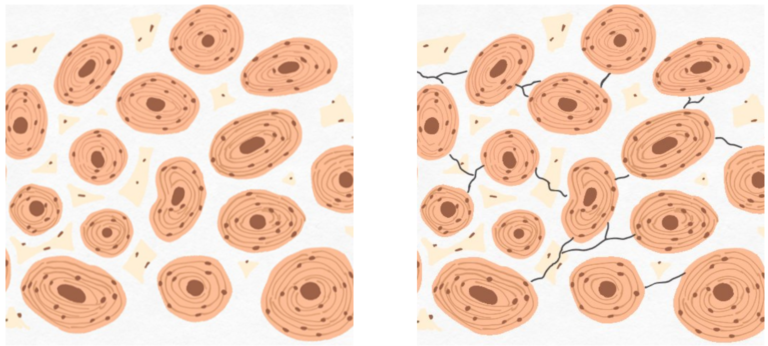

(a) (b)

Figure 3: (a) Osteons in an intact state, (b) Osteon system with micro-cracks.

[24, 25, 26]. Applied to this context, the Percolation Theory deals with the probability p of cracking of the net bonds and the critical probability p_c of percolation, meaning the complete propagation of the crack from end to end of the net.

The most common percolation model is a model where the bonds are independently percolated according to a Bernoulli stochastic process: the probability p of a bond to be cracked does not depend on the cracking of neighboring bonds, and is homogeneous across the net of bonds (so p does not depend on the level of stress or other factors at each point). For modeling mechanical fracture, the Bernoulli independent percolation model is not very realistic and needs an adequate generalization: either associating the percolation probability p to the non-homogeneous stress field or including some other type of dependence among the percolation of neighboring bonds. For this reason, a new percolation model is proposed.

Because bone can be treated as an almost brittle material, the cracking of a bond can be described commonly by a Weibull probability distribution [35, 36]. Due to this, we propose a non-independent percolation model where the percolation probability of a bonding is a function of the local stress:

$$p(\sigma; \sigma_0, \alpha) = 1 - e^{-(\sigma/\sigma_0)^{\alpha}} \tag{2}$$

The above formula defines a Weibull distribution, being σ the bond stress, σ_0 the scale parameter of the Weibull distribution, and α the shape parameter. In previous studies of the literature of ceramics and biomaterials [36, 37, 38], most authors provided values of $\alpha \approx 4$ and being $\alpha = 4$ the limit value between both types of materials, for this reason, the proposed model uses this value. This value is verified in the results section, showing that small deviations from $\alpha = 4$ exhibit no significant changes in the behavior of the model. On the other hand, σ_0 is a parameter that can be fitted for each rib analyzed from the vertical asymptote $\sigma = \sigma_\infty$ determined experimentally from the hits-stress curve of each rib, as:

$$\sigma_\infty = \sigma_0 \ln^{1/\alpha}\left(\frac{1}{1 - p_c}\right) \tag{3}$$

where p_c is the critical percolation probability that in a basic orthogonal mesh is $p_c = 1/2$ [39].

When the net tends to the complete percolation (completely cracked state), the probability of percolation p of the bonds tends to the critical probability p_c, and the size of the greatest cluster of cracked bonds $\#\mathcal{C}_0$ grows according to a law independent of the shape of the network. It is assumed that for each cracking of a bond, there is an AE signal, so the total number of AE detected (N_{AE}) growths proportionally to the predicted size $\#\mathcal{C}_0$. The Percolation theory estimates this number as:

$$N_{AE} \propto \#\mathcal{C}_0 \propto \frac{1}{|p - p_c|^\gamma} \tag{4}$$

being γ the universal critical exponent (which is independent of the net shape). By introducing equations (2) and (3) in equation (4), this leads to:

$$N_{AE} = \frac{n_0}{\left|(1 - p_c) - \exp\left[\left(\frac{\sigma}{\sigma_\infty}\right)^\alpha \ln(1 - p_c)\right]\right|^\gamma} \tag{5}$$

where n_0 is a proportionality parameter whose value is different for each rib. Thus, equation (5) predicts the stress behavior of the rib based on the hits or AE signals detected on the specimen and the fracture propagation, where N_{AE} and σ are the experimental values, $p_c = 1/2$ and $\alpha = 4$ are prescribed values and n_0, γ and σ_∞ are the parameters to be fitted.

3 Results

A set of 15 complete human ribs were tested under three-point bending to complete fracture, incorporating the AE technique. The stress-strain curves of the fracture section of some ribs are shown in Figure 4.

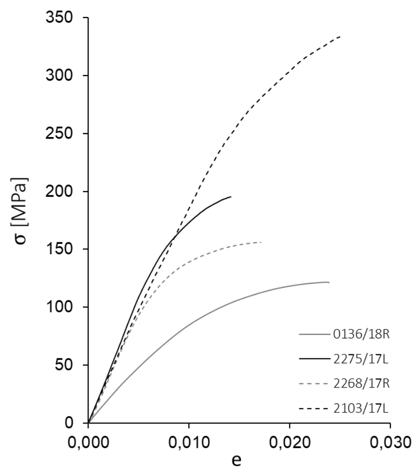

Figure 4: Stress-strain curves of rib bending tests.

As shown in Figure 5, hits are mainly detected at high stress levels where irreversible damage appears. From the set of tests, it is observed that the signals occur from the 45% of the maximum stress, where in most ribs, the 80% of the hits appear in the range of 75−100% of the stress fracture (see Figure 5). This concentration of hits at high stress levels results in a clear vertical asymptote of hits at maximum stress values.

The model proposed in equation (5) was fitted to the stress-hits data obtained from the tests, as shown in Figure 5. For the fittings, values of $\alpha = 4$ and $p_c = 1/2$ were assumed, while the parameters n_0, γ and σ_∞ were obtained for each rib by a fitting procedure. By means of a second fitting based on the parameters obtained, it was confirmed that $\alpha \approx 4$ is a reasonable guess.
Once the parameters were obtained, a more detailed analysis was carried out to determine the influence of the anthropometric factors in the parameters and the mechanical properties by means of Linear Regression Analysis (LRA) and Analysis of Variance (ANOVA).

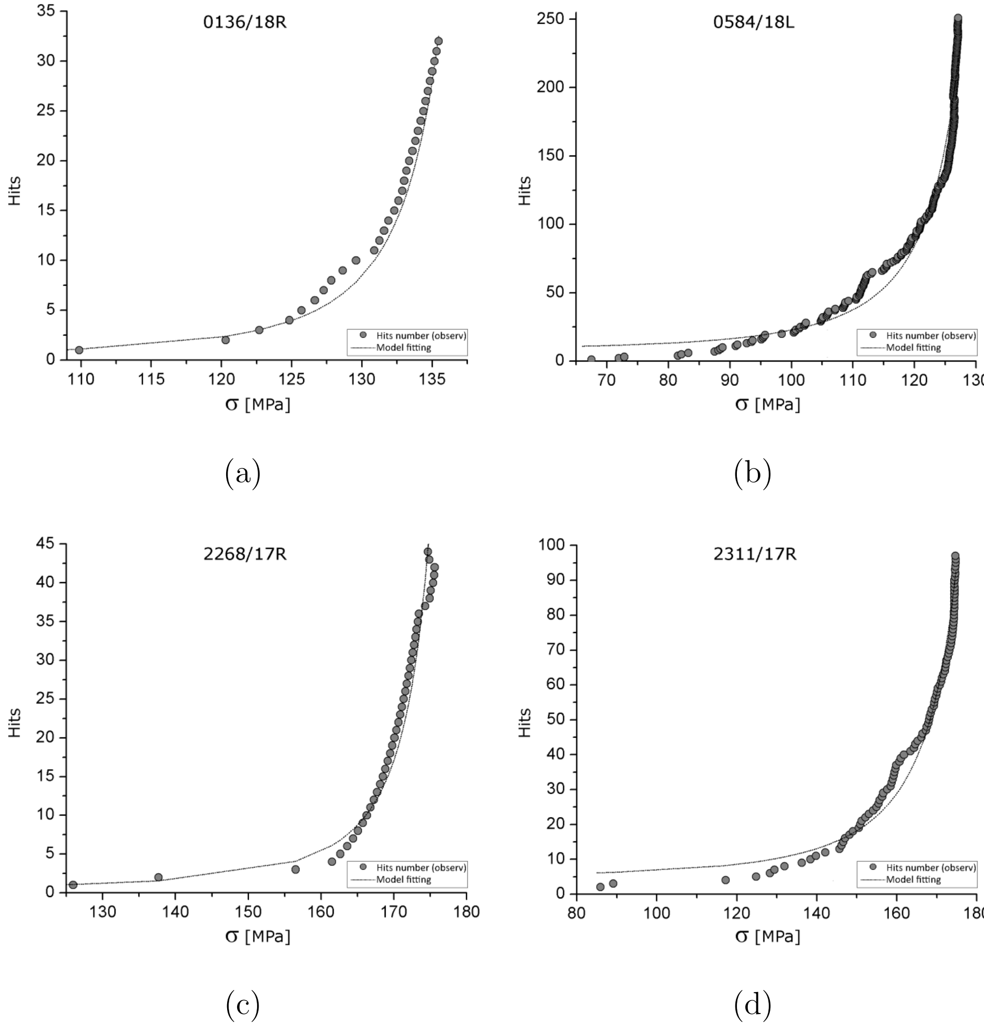

Figure 5: *Hits*-stress plot (dots) of rib bending tests detected by the AE technique and model fitting (line). Hits are concentrated at high stress levels in a clear asymptote.

As expected, the vertical asymptote stress σ_∞ showed to be statistically correlated with age ($p = 0.002$), showing a decrease in older subjects. A decrease in the scale parameter n_0 with increasing age ($p = 0.0160$) was also attested. Nevertheless, the critical percolation exponent γ showed to be relatively constant between the specimens and in a range of $1.80 \leq \gamma \leq 2.40$. No influence of any variable was seen in this parameter.

Table 1: Parameters obtained from fitting the model to the experimental data of hits and stress.

Rib	σ_∞	n_0	γ	λ	Rib	σ_∞	n_0	γ	λ
0136/18L	165	0.338	2.32	0.329	**2268/17L**	185	0.712	1.89	0.370
0136/18R	142	0.061	2.28	—	**2268/17R**	183	0.128	2.07	0.354
0182/18L	156	0.110	2.10	0.341	**2273/17L**	168	1.045	1.95	0.332
0182/18R	180	0.400	2.10	0.328	**2273/17R**	180	0.600	1.89	—
0520/18L	310	1.508	1.89	—	**2275/17L**	189	0.530	1.80	0.268
0584/18L	139	2.156	2.12	0.325	**2311/17L**	191	1.472	1.91	0.286
2102/17L	200	0.480	2.43	0.380	**2311/17R**	198	2.400	1.80	0.336
2103/17L	325	1.900	1.80	—					

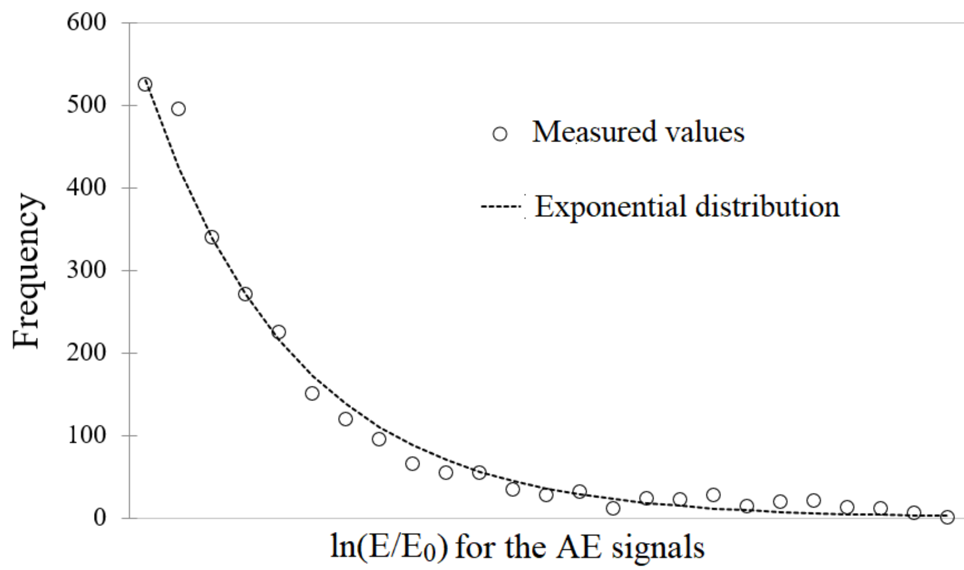

Figure 6: Comparison of the total observed number of hits (circles) and an exponential distribution (dotted line).

Finally, the experiments were also used to examine other hypotheses that fell outside the proposed model. For example, it is a well-known fact that intensities and energies of the AE signals follow well-known distributions [21, 20]. In particular, many authors have found that the energy of AE signals are distributed according to a power law of this type:

$$\mathbb{P}(\text{energy an AE signal} \leq E) = 1 - \left(\frac{E_0}{E}\right)^{\lambda} \tag{6}$$

where $\mathbb{P}$ refers to a probability, $\lambda > 0$ is the exponent of the power law, and E_0 is the threshold energy (lower energy signals are ignored since they correspond to phenomena other than micro-cracking, so $E \geq E_0$). By defining the logarithmic variable $U = \ln(E/E_0)$, one has that the new variable U is distributed according to an exponential distribution with probability density function given by:

$$p_U(u) = \lambda e^{-\lambda u} \tag{7}$$

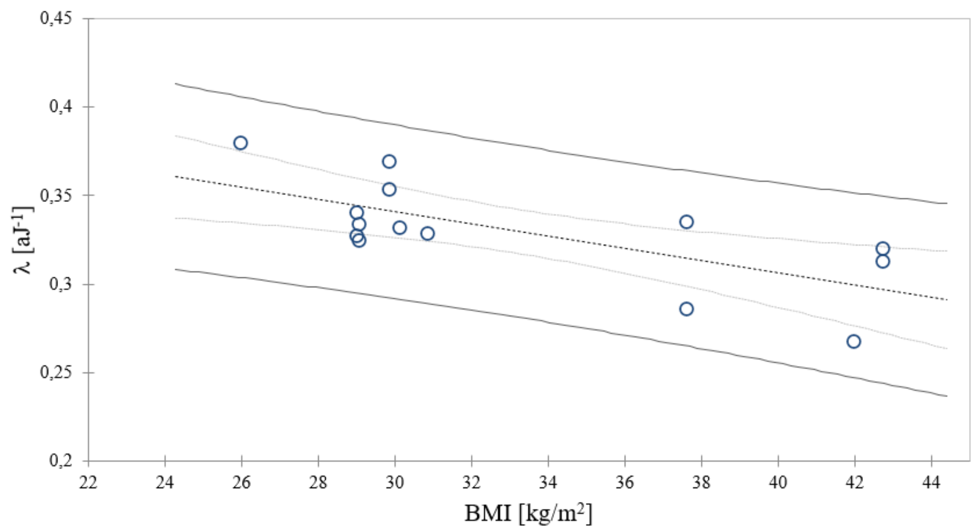

Figure 7: Scatter plot of the power-law parameter λ for the distribution of AE energies and BMI.

This is precisely what is observed in the measured energy of the AE signals whose distribution is shown in Figure 6. In Table 1, the values of λ for all the samples with a sufficiently large number of hits N are given (when N is not large, the error in λ is significant, and there is not a good fitting to an exponential distribution). It is interesting to note that, unexpectedly, λ seems to be very significantly correlated with the Body Mass Index (BMI) of the individuals (p-value < 0.005), see Figure 7. Previous analysis showed that there was not a significant relation between age and BMI (p-value = 0.162).

4 Discussion

In this paper, it has been proposed a model for the prediction of the onset of micro-cracking related to the beginning of irreversible damage and prior to the macroscopic fracture, based on the Percolation Theory. For this purpose, whole human rib bending tests were performed, incorporating the AE sensors during the tests. Experimental data were used to fit the model parameters and to show the model behavior.

Some existing models describe the succession of AE signals by assuming a pre-imposed power law, trying to fit the sudden increase of hits or AE signals once achieved certain pressure level near the maximum pressure [40]; the same power law is found for biological tissues [20, 21]. In any case, different explanations have been proposed for the occurrence of power laws, from models based on viscoplasticity [41] to explanations based on Percolation Theory.

Micro-cracking is a stochastic process controlled by different factors and, for this reason, it involves some kind of randomness. This randomness seems to be associated with microscopic details in micro-structure both in biological materials and in non-biological materials. In biological tissue the microstructure is influenced by anthropometric factors [42]. However, as the AE demonstrates, the fracture process occurs progressively, where micro-cracks propagate through the microstructure until the main fracture completely crosses the material. This process can be studied based on the Percolation Theory of bonds (analogous to the cement lines and interstitial bone between osteons), which progressively break.

As shown in Figure 5, the ideas of the Percolation Theory predict that there will be an asymptotic behavior in the number of detected AE signals. Furthermore, the approximation to the asymptote is given by a universal exponent γ whose values are close to the values predicted by the independent Percolation Theory. In 2D percolation, the expected value of the exponent is $\gamma \approx 2.38$, while 3D percolation, it is $\gamma \approx 1.80$ [43, 44]. Although we have a

plane stress state, when the crack appears, the symmetry is broken, and this is reason why we would expect values in the range $1.80 \leq \gamma \leq 2.38$ as it indeed happens: $\gamma = 2.023 \pm 0.22$. The expected values correspond to independent Bernoulli percolation, but in the present case, the bond breakages are not independent nor the probability is homogeneous, which would also make us expect some deviation with respect to the theoretical value for the exponents γ. Indeed, this is a limitation of the study since the mathematical problem of finding the values for a non-independent percolation process depending on a stress field is still an open problem [45, 46].
On the other hand, the parameter n_0 shows a great variability, but it exhibits a significant descent with age (p-value $= 0.016$). Also, the parameter σ_∞ shows a significant decrease with age (p-value $= 0.0002$), which is not a surprise, since the parameter is essentially the failure stress, and it is well known that this magnitude decreases with age [47].

Another virtue of the proposed model is the prediction/anticipation of structural failure. As the hits occur, it would be possible with each new hit to re-evaluate the expected value σ_∞ for the failure stress that appears in the equation (3). If the quotient between the current stress and that σ/σ_∞ value is close enough to 1, we could conjecture that we are close to complete failure even without getting too close to it, which could have several applications as a potentially usable method to anticipate mechanical failure from the evidence of accumulated micro-cracks.

5 Conclusion

Using some ideas of the Percolation Theory, we have proposed a model that is able to quantitatively describe the distribution of AE signals as stress on cortical bone increases. This model could be used in practical situations to anticipate structural failure of the human rib subjected to bending. The model provides a reasonable fit, and the results show that the model parameters exhibit consistency with the two exponents of the Percolation Theory. Moreover, it has been found that some parameters appear to correlate with anthropometric variables (age and BMI), suggesting that this model is able to capture some influence of these factors on bone microstructure.

Besides, the energy distribution of the AE signals has been examined, and it has been found that an exponent determining its distribution appears to be significantly correlated with the subject's BMI, which is a promising finding because it suggests that there is a correlation between BMI and microstructure of human cortical bone.

References

[1] Karali, A., Kao, A. P., Meeson, R., Roldo, M., Blunn, G. W., & Tozzi, G. (2020). "Full-field strain of regenerated bone tissue in a femoral fracture model". *Journal of Microscopy*, **29**(4), pp. 373–380.

[2] Van den Munckhof, S., & Zadpoor, A. A. (2014). "How accurately can we predict the fracture load of the proximal femur using finite element models?". *Clinical Biomechanics*, **29**(4), pp. 373–380.

[3] Lentle, B. C., Aldrich, J. E., & Akhtar, A. (2000). U.S. Patent No. 6,024,711. Washington, DC: U.S. Patent and Trademark Office.

[4] Shrivastava, S., & Prakash, R. (2009). "Assessment of bone condition by acoustic emission technique: A review". *Journal of Biomedical Science and Engineering*, **2**(3), pp. 144.

[5] Agcaoglu, S., Akkus, O. (2013). "Acoustic emission based monitoring of the microdamage evolution during fatigue of human cortical bone". *Journal of biomechanical engineering*, **135**(8), pp. 081005.

[6] Kapur, R. A. (2016). "Acoustic emission in orthopaedics: A state of the art review". *Journal of biomechanics*, **49**(16), pp. 4065-4072.

[7] Browne, M., Roques, A., & Taylor, A. (2005). "The acoustic emission technique in orthopaedics-a review". *The Journal of Strain Analysis for Engineering Design*, **40**(1), pp. 59-79.

[8] Hirasawa, Y., Takai, S., Kim, W. C., Takenaka, N., Yoshino, N. & Watanabe, Y. (2002). "Biomechanical monitoring of healing bone based on acoustic emission technology". *Clinical Orthopaedics and Related Research (1976-2007)*, **402**, pp. 236-244.

[9] Agelis, D., Blom, J., De Sutter, S., Verbruggen, S., Strantza, M., Tysmans, T. & Nguyen, P. (2016) "Fracture monitoring by acoustic emission: recent applications of parameter-based characterization". *9th International Conference on Fracture Mechanics of Concrete and Concrete Structures*.

[10] Carpinteri, A., Lacidogna, G., Accornero, F., Mpalaskas, A.C., Matikas, T.E. & Aggelis, D.G. (2013) "Influence of damage in the acoustic emission parameters". *Cement and Concrete composites*, **44**, pp. 9–16.

[11] Hanagud, S., Clinton, R.G., Chouinard, M.D., Berg, E. & Nichols, P.J. (1977) "Soft tissues and acoustic emission based diagnostic tools". *Ultrasonics Symposium*, pp. 242–246.

[12] Huang, M., Jiang, L., Liaw, P.K., Brooks, C.R., Aeeley, R. & Klarstrom, D.L. (1998) "Using acoustic emission in fatigue and fracture materials research". *JOM*, **50**(11) pp. 1–14.

[13] Franke, R.P., Dorner, P., Schwalbe, H.J. & Ziegler, B. (2004) "Acoustic emission measurement system for the orthopedic diagnosis of the human femur and knee joint". *Journal of Acoustic Emission*, **22** pp. 236–242.

[14] Strantza, M., Polyzos, D., Louis, O., Boulpaep, F., Van Hemelrijck, D. & Aggelis, D.G. (2015) "Damage characterization on human femur bone by means of ultrasonics and acoustic emission". *Journal of Physics: Conference Series*, **628** pp. 12–16.

[15] Aggelis, D., Strantza, M., Louis, O., Boulpaep, F., Polyzos, D. & Van Hemelrijck, D. (2015) "Fracture of human femur tissue monitored by acoustic emission sensors". *Sensors*, **15**(3) pp. 5803–5819.

[16] Watanabe, Y., Takai, S., Arai, Y., Yoshino, N. & Hirasawa, Y. (2001) "Prediction of mechanical properties of healing fractures using acoustic emission". *Journal of Orthopaedic Research*, **19**(4) pp. 548–553.

[17] Hanagud, S., Clinton, R.G. & Lopez, J.P. (1973) "Acoustic emission in bone substance". *Proceedings of Biomechanics Symposium of the American Society of Mechanical Engineers, ASME*, **74**.

[18] Netz, P. (1979) "The diaphyseal bone under torque: an experimental study on dogs". *Acta Orthopaedica Scandinavica*, **50**(176) pp. 1–32.

[19] Fischer, R. A., Arms, S. W., Pope, M. H. & Seligson, D. (1986) "Analysis of the effect of using two different strain rates on the acoustic emission in bone". *Journal of biomechanics*, **19**(2) pp. 119–127.

[20] Baró, J., Shyu, P., Pang, S., Jasiuk, I. M., Vives, E., Salje, E. K. & Planes, A. (2016) "Avalanche criticality during compression of porcine cortical bone of different ages". *Physical Review E*, **93**(5) pp. 053001.

[21] Sánchez-Molina, D. and Martínez-González, E. and Velázquez-Ameijide, J. and Llumà, J. and Soria, M. R. & Arregui-Dalmases, C. (2015). "A stochastic model for soft tissue failure using acoustic emission data". *Journal of the mechanical behavior of biomedical materials*, **51**, pp. 328–336.

[22] García Vilana, S., Martínez González, E., Sánchez Molina, D., Arregui Dalmases, C., Velázquez-Ameijide, J. & Llumà Fuentes, J., Rebollo Soria, M. C. (2016). "Aplicación de la emisión acústica como método para anticipar el fallo de tejidos colaginosos (1ª parte)". *Revista de la Asociación Española de Ensayos No Destructivos*, **77**, pp. 28–34.

[23] García Vilana, S., Martínez González, E., Sánchez Molina, D., Arregui Dalmases, C., Velázquez-Ameijide, J. & Llumà Fuentes, J., Rebollo Soria, M. C. (2016). "Aplicación de la emisión acústica como método para anticipar el fallo de tejidos colaginosos (2ª parte)". *Revista de la Asociación Española de Ensayos No Destructivos*, **78**, pp. 24–31.

[24] Sasaki, N., Yamamura, H, & Matsushima, N. (1986). "Is there a relation between bone strength and percolation?". *Journal of theoretical biology*, **122**(1), pp. 25–31.

[25] Pfretzschner, Hans-Ulrich (2000). "Percolation theory relates corticocancellous architecture to mechanical function in vertebrae of inbred mouse strains". *Neues Jahrbuch für Geologie und Paläontologie-Abhandlungen*, pp. 413–432.

[26] Tommasini, S.M., Wearne, S.L., Hof, P.R., Jepsen, K.J. (2008). "Is there a relation between bone strength and percolation?". *Bone*, **42**(4), pp. 743–750.

[27] Liu, J.-P., Li, Y.-H., Yang, Y.-J. (2010). "Study on characteristics of percolation in rock failure process via acoustic emission locating technique". *Journal of Northeastern University (Natural Science)*, **12**, pp. 26.

[28] Lysak, M. V. (1994) "Acoustic emission during jumps in subcritical growth of cracks in three-dimensional bodies". *Engineering fracture mechanics*, **47**(6), pp. 873–879.

[29] Cook, R. D., & Young, W. C. (1999). *Advanced mechanics of materials*, Upper Saddle River, NJ: Prentice Hall.

[30] Caiero, J.R., González, P. & Guede, D. (2013) "Biomecánica y hueso (y II): Ensayos en los distintos niveles jerárquicos del hueso y técnicas alternativas para la determinación de la resistencia ósea". *Revista de osteoporosis y metabolismo mineral*, **5**(2), pp. 99–108.

[31] Guo, X.E., Liang, L.C. & Goldstein, S.A. (1998) "Micromechanics of osteonal cortical bone fracture". *Journal of Biomechanical Engineering*, **120**, pp. 112–117.

[32] O'Brien, F.J., Taylor, D. & Lee, T.C. (2005) "The effect of bone microstructure on the initiation and growth of micro-cracks". *Journal of Orthopaedic Research*, **23**(2), pp. 475–480.

[33] Najafi, A.R., Arshi, A.R., Eslami, M.R., Fariborz, S. & Moeinzadeh, M.H. (2007) "Micromechanics fracture in osteonal cortical bone: A study of the interactions between micro-crack propagation, microstructure and the material properties". *Journal of Biomechanics*, **40**(12), pp. 2788–2795.

[34] Wang, M., Zimmermann, E.A., Riedel, C., Busseb, B., Li, S. & Silberschmidt, V.V. (2017) "Effect of micro-morphology of cortical bone tissue on fracture toughness and crack propagation". *Procedia Structural Integrity*, **6**, pp. 64–68.

[35] Basu, B., Tiwari, D., Kundu, D., Prasad, R. (2009). " Is Weibull distribution the most appropriate statistical strength distribution for brittle materials?". *Ceramics International*, **35**(1), pp. 237–246.

[36] Bertalan, Z., Shekhawat, A., Sethna, J. P., Zapperi S. (2014). "Fracture strength: stress concentration, extreme value statistics, and the fate of the Weibull distribution". *Physical Review Applied*, **2**(3), pp. 034008.

[37] Menig, R., Meyers, M.H., Meyers, M.A., Vecchio, K.S. (2000). "Quasi-static and dynamic mechanical response of Haliotis rufescens (abalone) shells". *Acta materialia*, **48**(9), pp. 2383–2398.

[38] Tinschert, J., Zwez, D., Marx, R., Anusavice, K.J. (2000). "Structural reliability of alumina-, feldspar-, leucite-, mica-and zirconia-based ceramics". *Acta materialia*, **28**(7), pp. 529–535.

[39] Parviainen, Robert (2007). "Estimation of bond percolation thresholds on the Archimedean lattices". *Journal of Physics A*, **40**(31), pp. 9253–9258.

[40] Johansen, A., & Sornette, D. (2000). "Critical ruptures". *The European Physical Journal B-Condensed Matter and Complex System*, **18**(1), pp. 163–181.

[41] Weiss, J., Lahaie, F., & Grasso, J. R. (2000) "Statistical analysis of dislocation dynamics during viscoplastic deformation from acoustic emission". *Journal of Geophysical Research: Solid Earth*, **105**(B1), pp. 433–442.

[42] Velázquez-Ameijide, J., García-Vilana, S., Sánchez-Molina D, Llumà-Fuentes, J., Martínez-González, E., Rebollo-Soria, M.C., & Arregui-Dalmases, C. (2020): "Prediction of mechanical properties of human rib cortical bone using fractal dimension". *Computer Methods in Biomechanics and Biomedical Engineering*, 1–11.

[43] Gaunt, D. S., & Ruskin, H. (1978): "Bond percolation processes in d dimensions". *Journal of Physics A*, **11**(7), pp. 1369.

[44] Adler, J., Meir, Y., Aharony, A., & Harris, A. B. (1990): "Series study of percolation moments in general dimension". *Physical Review B*, **41**(13), pp. 9183.

[45] Gandolfi, A., Keane, M. S., & Newman, C. M. (1992): "Uniqueness of the infinite component in a random graph with applications to percolation and spin glasses". *Probability Theory and Related Fields*, **92**(4), pp. 511–527.

[46] Gaboriau, D. (2005): "Invariant percolation and harmonic Dirichlet functions". *Geometric & Functional Analysis*, **15**(5), pp. 1004–1051.

[47] Velázquez-Ameijide, J., García-Vilana, S., Sánchez-Molina, D., Martínez-González, E., Llumà, J., Rebollo-Soria, M. C., & Arregui-Dalmases, C. (2021). "Influence of anthopometric variables on the mechanical properties of human rib cortical bone". *Biomedical Physics & Engineering Express*, **7**(3), 035013.